

DMR

89-1

6-1

**VIRGINIA DIVISION OF MINERAL RESOURCES
OPEN-FILE REPORT 89-1**

**EVALUATION OF SEDIMENT DYNAMICS AND THE MOBILITY OF
HEAVY MINERALS ON THE VIRGINIA INNER CONTINENTAL SHELF**

John D. Boon and C. R. Berquist, Jr.

COMMONWEALTH OF VIRGINIA
DEPARTMENT OF MINES, MINERALS AND ENERGY
DIVISION OF MINERAL RESOURCES
R. C. Milici, Commissioner of Mineral Resources and State Geologist

CHARLOTTESVILLE, VIRGINIA
August, 1989

Department of Mines, Minerals and Energy
Richmond, Virginia
O.Gene Dishner, Director

Copyright 1989, Commonwealth of Virginia

Evaluation of Sediment Dynamics and the Mobility of
Heavy Minerals on the Virginia Inner Continental Shelf

by

John D. Boon
Virginia Institute of Marine Science
and School of Marine Science
College of William and Mary
Gloucester Point, Virginia 23062

C. R. Berquist, Jr.
Virginia Department of Mines, Minerals and Energy
Division of Mineral Resources
Charlottesville, Virginia 22903

The work reported herein was funded in part by the Minerals Management Service, United States Department of the Interior, under Federal Grant No. 14-12-0001-30296 to the Bureau of Economic Geology, The University of Texas at Austin, Austin, Texas.

CONTENTS

	Page
Abstract	1
Introduction	1
Field experiments	1
Instrumentation	5
First deployment	5
Bottom description	5
Second deployment	6
Data Analysis	6
Averaged currents	6
Wave statistics	6
Bottom orbital velocities	11
Initial sediment motion	11
Interpretation of Results	14
Sediment motion induced by waves	14
Sediment resuspension layer	17
Potential sediment transport due to currents	17
Heavy mineral enrichment	20
Heavy minerals found in suspension	20
References	21
Appendix A: Bottom sediment grain size analyses	23
Appendix B: Suspended sediment mineral composition	26

ILLUSTRATIONS

	Page
Figure	
1. Regional map showing the approximate locations of Smith Island Shoal	2
2. Benthic boundary layer tripod being deployed	3
3. Section of NOS chart 12221	4
4. Vector diagram of hourly mean bottom current at site A	7
5. Vector diagram of hourly mean bottom current at site B	8
6. Vector diagram of hourly mean bottom current at site C	9
7. Vector diagram of hourly mean bottom current at site C	10
8. Scattergram of wave orbital velocities	12
9. Combined wave and current in the direction of wave advance, site B	13
10. Critical velocity for initial grain motion	15
11. Combined wave and current in direction of wave advance, site C	16
12. Plot of suspended sediment concentration at five elevations	18
13. Profiles of suspended sediment concentration	19

TABLE

1. Comparison of average composition of sediment from different environments	21
--	----

EVALUATION OF SEDIMENT DYNAMICS AND THE MOBILITY OF HEAVY MINERALS ON THE VIRGINIA INNER CONTINENTAL SHELF

ABSTRACT

Two benthic instrumented tripods were deployed in the summer and fall of 1987 at Smith Island Shoal, a coastal-parallel sand ridge situated just north of the Chesapeake Bay entrance on the Virginia inner shelf. Previous studies of the shoal have noted a high abundance of heavy minerals (up to 16 percent by weight) contained within the surficial sediments (fine to very fine sands) along its flanks as compared to much lower concentrations elsewhere. It is unknown whether this high abundance is due to existing hydrodynamic factors (selective entrainment), exhumation of relic deposits, or some other cause.

Our measurements of near-bottom current, wave-orbital velocity, wave height (pressure) and optically-sensed suspended sediment concentration at 5 positions within a meter of the bed reveal that the heavy mineral enriched flank areas of the shoal frequently experience wave-induced bottom orbital velocities well in excess of the critical level needed to produce grain motion. During periods of moderate wave activity ($H_{mo} = 0.8 - 1.0$ m, $T = 8.5 - 9.5$ s) bottom orbital velocities were "groupy" in their distribution, reaching maximum values as high as 60 cm/s. Suspended sediment concentration values averaged at 8-s intervals revealed strong, periodic resuspension of bed material at wave-group time scales less than 1 meter above the bed. Trapped samples of the suspended material show approximately the same mineral composition as that of the local bed material. While wave-induced resuspension of heavy minerals into the water column is thus indicated during all but fairweather conditions, we observed that near-bottom steady currents were erratic and generally small compared to those normally expected near a major coastal embayment entrance. Our evidence suggests that a wave-dominated environment prevails with little potential for a sediment transport pathway and selective mineral sorting.

INTRODUCTION

This report describes the benthic environment and near-bed fluid dynamics of a selected sand-ridge feature located at Smith Island Shoal, approximately 7.5 nautical miles east of Smith Island Inlet on the Virginia inner continental shelf (Figure 1). Interest in this feature derives from its previous identification as a point of local enrichment in heavy mineral concentrations within the bottom sediment. A prior report (Berquist and Hobbs, 1986), noted concentrations as high as 16 percent (averaging 8 percent) of total sample weight for those minerals with a specific gravity in excess of 2.85 in the area of the shoal. Specifically, the enriched material was found within a surface layer of fine to very fine sand deposited on the flanks and within the troughs of two sand ridges having a maximum topographic relief of about 2 meters in depths averaging about 10 meters. The crest of the central ridge of Smith Island Shoal contains coarse sand with few heavy minerals. Stubblefield and others (1975) and Swift (1976) have described similar ridge features in New Jersey at 10-meter depths, noting fine to very fine sand on ridge flanks and coarse crestal sands thought to be a winnowing response to wave surge.

Given this background, the present investigation seeks to characterize the dynamics of the benthic boundary layer at the Smith Island Shoal site and determine the extent of its influence on the mobility (entrainment and subsequent transport) of the light and heavy mineral fractions located at the sediment-water interface. Research at this stage has focused on the relative ability of wave and tide-induced steady flows and wave-induced oscillatory flow to initiate entrainment and transport of sediment grains of different density. Determining the extent to which high-density minerals participate in such transport is an initial step toward answering the question of how heavy mineral enrichment may have occurred; i.e., through local hydraulic processes now active on the inner shelf, as simple exhumation of an antecedent (ancient) deposit during long-term shoreface retreat or shoreline adjustment, or due to some other cause.

FIELD EXPERIMENTS

Two separate field experiments were conducted involving two automated, bottom-mounted boundary layer instrumentation systems (Figure 2). The electronic components of these systems are mounted on tubular aluminum tripods fitted with lead support disks at their base so that they rest in a stable position on the sea bed while collecting data. In their basic configuration, each tripod is designed to obtain direct measurements of near-bottom orbital velocity and suspended sediment concentration, in addition to surface wave data and samples of the sedimentary material found in suspension near the bed.

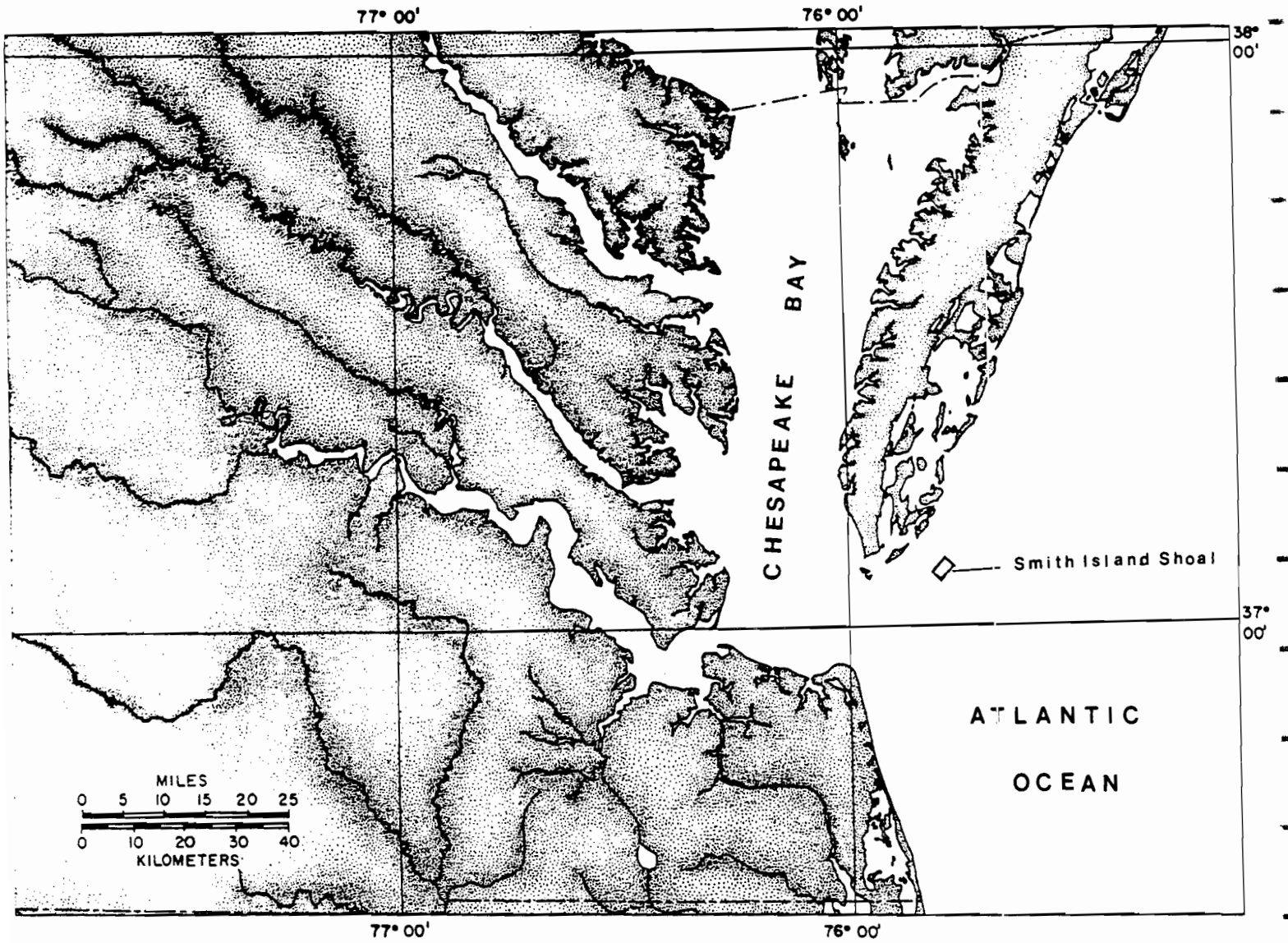


Figure 1. Regional Map showing the approximate location of Smith Island Shoal on the Virginia inner shelf.

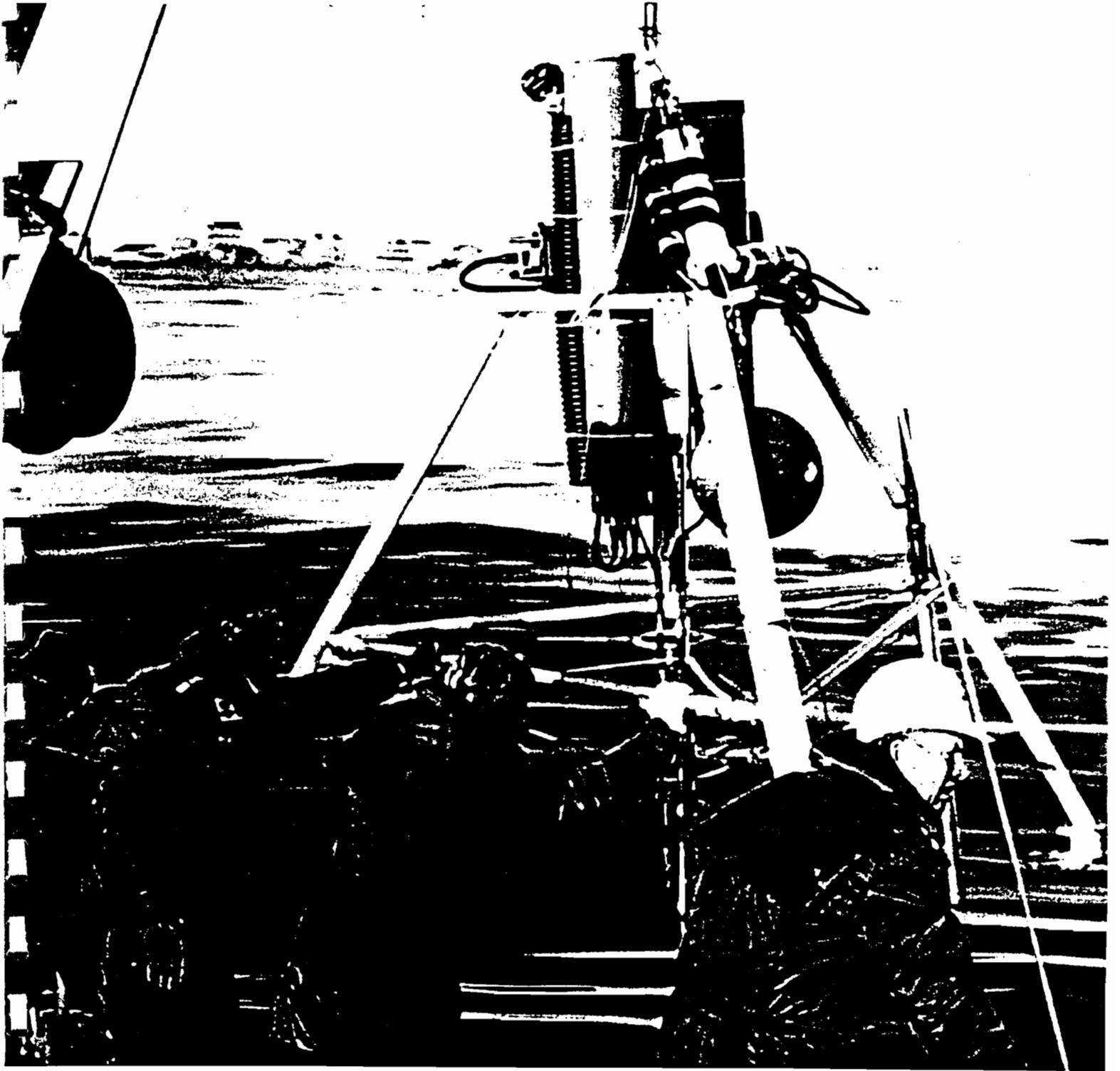


Figure 2. Benthic Boundary Layer Tripod being deployed.

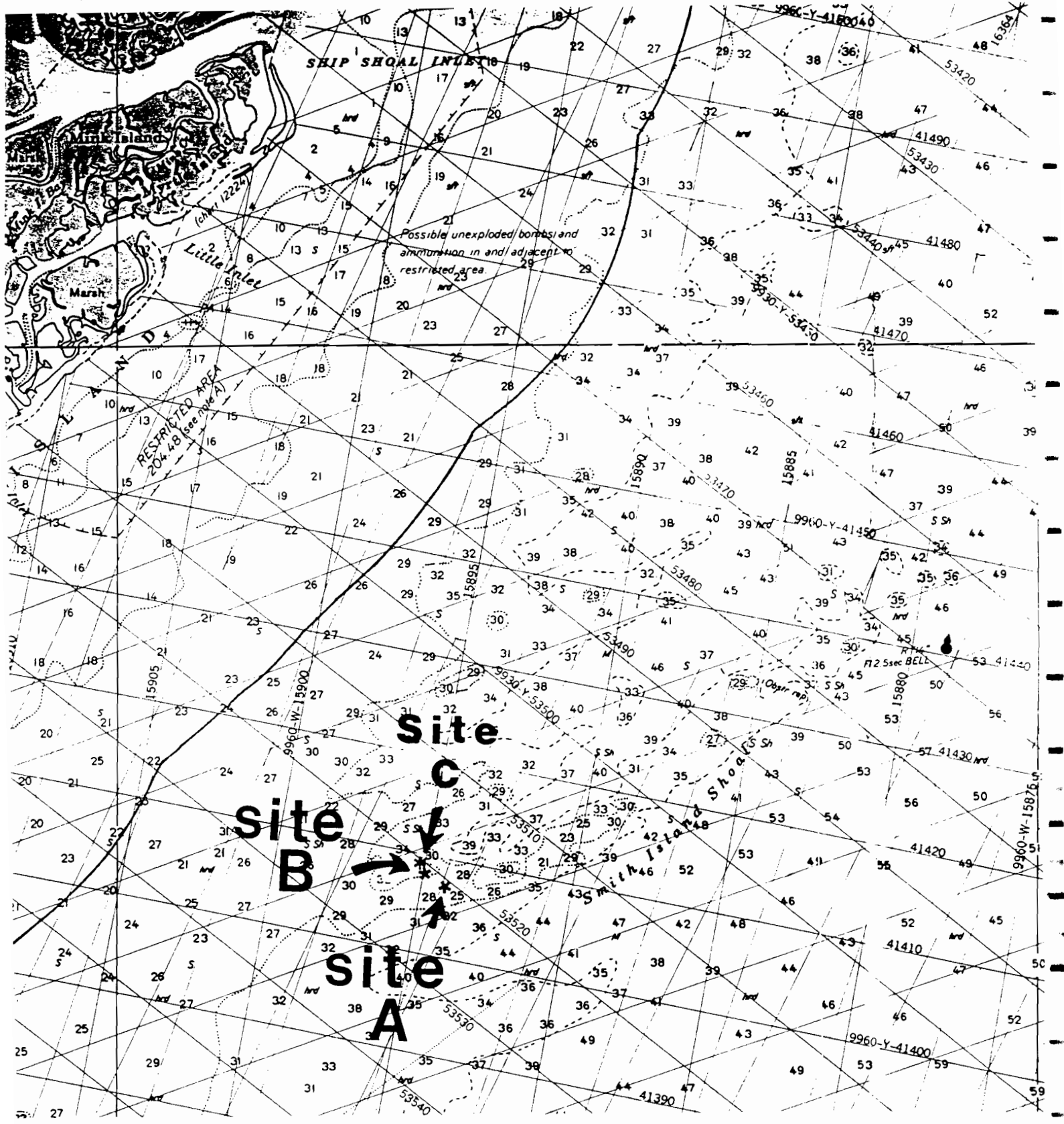


Figure 3. Section of NOS chart 12221 showing location of tripod deployment sites A, B and C and bathymetric detail.

INSTRUMENTATION

The primary instrument on both of the tripods described above is a Sea Data model 635-9RS directional wave gauge and current meter with burst sampling capability. Sampling in a "burst" mode allows a pre-selected number of rapid measurements (e.g., 1024 samples taken at 1-second intervals for a total burst duration of 17.1 minutes) to be collected at a longer, preset burst interval (once every hour in the present case). The 635-9RS measures horizontal flow using a two-axis Marsh-McBirney model 512 electromagnetic current meter with a 4.0-cm spherical sensor element. All EM sensors used in our experiments are individually calibrated in the VIMS re-circulating flume and have individual gain and offset constants. These are applied to each sensor during conversion of the raw data into standard engineering units by linear regression formula. A typical r.m.s. standard deviation from regression was found to be ± 1.0 cm/s in the range 0 to 70 cm/s. Pressure measurements (millibars) are obtained on the 635-9RS using a Paroscientific, Inc. digi-quartz transducer yielding 0.01 percent accuracy. The latter readings are converted to frequency-corrected sea surface elevations in meters above the bottom using a local frequency approximation method in combination with linear wave theory. The pressure sensor was positioned approximately 1.25 meters above the bed while the EM current sensor was located approximately 0.50 meters above the bed.

A second instrument used in the present field deployments measures suspended sediment concentration by optical means. A Downing Model OBS-2 sediment monitoring array was used with five infrared sensor-emitter elements spaced at logarithmic intervals above the bed starting at a height of 7 to 10 cm above the bottom. Sensing of sediment concentration is achieved by the "backscatterance" principle which yields a linear calibration curve for fine to medium sand suspensions and has the advantage of a small (approximately 3 cm) sensing distance allowing the units to operate very near to the bottom and to each other.

An integrated sample of the sediment in suspension near the OBS-2 array was obtained by means of a tubular sediment trap mounted on one corner of the tripod bearing that array. The trap consisted of two concentric cylinders, one mounted inside the other so as to permit sediment to collect between the inner and outer walls. Access to five vertically-segmented compartments of the tube was gained through a series of intake holes placed at the top of each compartment and below a plug forming the floor of the compartment above. The sediment collected thus represents a time-integrated sample covering the period of the deployment and is known to have reached a certain minimum height (the intake height of the corresponding compartment) during this time.

First Deployment

The first deployment involving a pair of benthic tripods began on the morning of August 17, 1987 at positions A and B shown in Figure 3. One tripod was placed on the bottom near the crest of the central ridge at a depth of approximately 9.8 meters below mean sea level (Site A, Figure 3). The second tripod was placed on the landward flank of the ridge in a water depth of approximately 10.4 meters below mean sea level (Site B, Figure 3). Both were left unattended on the sea floor until the morning of August 25, 1987. Tripod recovery was then accomplished by means of acoustic devices that release a small buoy carrying a cable to the surface after receiving a remote command signal.

A period of high winds and small craft warnings was experienced from about August 11 to August 15, 1987 shortly before the deployment. Winds blew steadily from the northeast at approximately 10-15 knots with higher gusts during this time before slackening to 5-10 knots from the southeast. At the time of deployment, surface winds were light and variable with a pronounced swell coming from the northeast. Winds remained light during the remainder of the deployment with light swell continuing its approach from the north to northeast direction.

Bottom Description

Divers inspected the two tripods to assure their correct orientation after reaching the bottom and to measure the height of the various sensors above the bed. Their visual observations also included a description of the bed at the time of deployment. At Site A (mean depth: 9.8 m), the bottom consisted of coarse brown sand forming long-crested ripples of 15 cm height and 60 to 70 cm wavelength. Surficial sand grains were everywhere experiencing a general oscillatory movement in response to the above-mentioned surface swell. Initial data records from the tripods show a significant wave height of 0.6 m with a wave period of 9.8 seconds at the time of deployment. At Site B (mean depth: 10.4 m), the bottom consisted of fine to very fine sand forming small ripples approximately 1.5 to 2 cm high with a 3 to 5 cm wavelength. Mixed with this surface sediment were numerous echinoderms ("sand dollars"), also observed in motion on the bed.

During removal of the tripods on August 25, divers reported roughly the same type of bedforms at both sites but the crests of the ripples were well-rounded, not sharp as they were initially. No sediments were observed in motion at this time.

Grain size analysis statistics for two surface sediment samples collected by divers at sites A and B are presented in Appendix A of this report. Mineral compositions for suspended sediment samples are given in Appendix B.

Second Deployment

A second field experiment was conducted during the period from October 16 through October 22, 1987 with a single instrumented tripod deployed at site C at approximately the same position as site B but at slightly greater depth. The October redeployment was undertaken for two principal reasons: 1) to obtain a record of bottom dynamic behavior less typical of fair-weather conditions than those of the August deployment, 2) to obtain optical measures of the suspended sediment concentration near the bed. Battery failure occurred in one of the recording instruments during the August deployment which negated the effort to obtain suspended sediment concentration data at that time.

Winds in excess of 10 knots were experienced during the initiation of the second deployment at site C. "Groupy" waves having a significant height of about 1 m and an average period of about 9 seconds were approaching from the northeast quadrant. This sea made the deployment more difficult than usual and divers could not be used to view the tripod on the bottom, in part due to highly turbid water and much reduced visibility compared to the first deployment.

DATA ANALYSIS

The data records collected by the Sea Data Model 635-9RS directional wave gauge and current meter units were processed to provide near-bottom simultaneous measures of fluid pressure (P) and two horizontal velocity vector components, U (positive eastward) and V (positive northward). These PUV measures were used in several ways.

Averaged Currents

By averaging the U,V velocity components over the burst duration (1024 seconds or 17.1 minutes), a resultant "steady" current vector was obtained with speed $R = \sqrt{U^2 + V^2}$ and direction $\Theta = \arctan(V/U)$. "Steady" means that the averaging period (17.1 minutes) is considered long with respect to the wave period (seconds) but short with respect to the tidal period (hours), thus eliminating the wave oscillatory motion only. These vector-averaged currents then represent the tidal flow near the bottom in combination with possible net flows from other sources (e.g., wind-induced coastal currents). The burst sampling interval used in our experiments (1 hour) is a suitable one for investigation of diurnal, semidiurnal and longer-period tidal and non-tidal flows. Two vector plots of averaged U,V components representing a 50-hour period during the August deployment at sites A and B are presented in Figures 4 and 5. Two separate 50-hour current plots are shown in Figure 6 and 7 for site C.

Wave Statistics

By plotting the individual (1 second) wave orbital velocity components on a U,V "scattergram", information was gained on the directional properties of the wave motion. The single digit appearing in each grid cell of the scattergram in Figure 8 represents the number of velocity vectors whose arrow "tips" extending from the central U,V origin have landed in that cell. Zeros are left blank while numbers in excess of 9 are indicated by an asterisk; the cell containing the vector average for the burst is indicated by the letter "A" in the center (centroid) of the scattered values. The ellipse formed by the contours of these directional density indices outlines the directional pattern of the dominant waves - dominant here in the sense of their impact on the bottom orbital velocity regime.

In the program used to generate the scattergram (developed by the senior author to run on an IBM-compatible PC computer), modal wave directions were computed in the following steps: the vector-averaged current was removed to obtain zero-mean wave orbital velocity components. These components were then referenced by a new set of coordinate axes (U',V'), rotated until maximum variance of the vector projections on the U' axis was obtained. The heading of the rotated U' axis (+ or - 180 degrees) was assumed indicative of the modal wave direction. Lastly, the U' vector components were

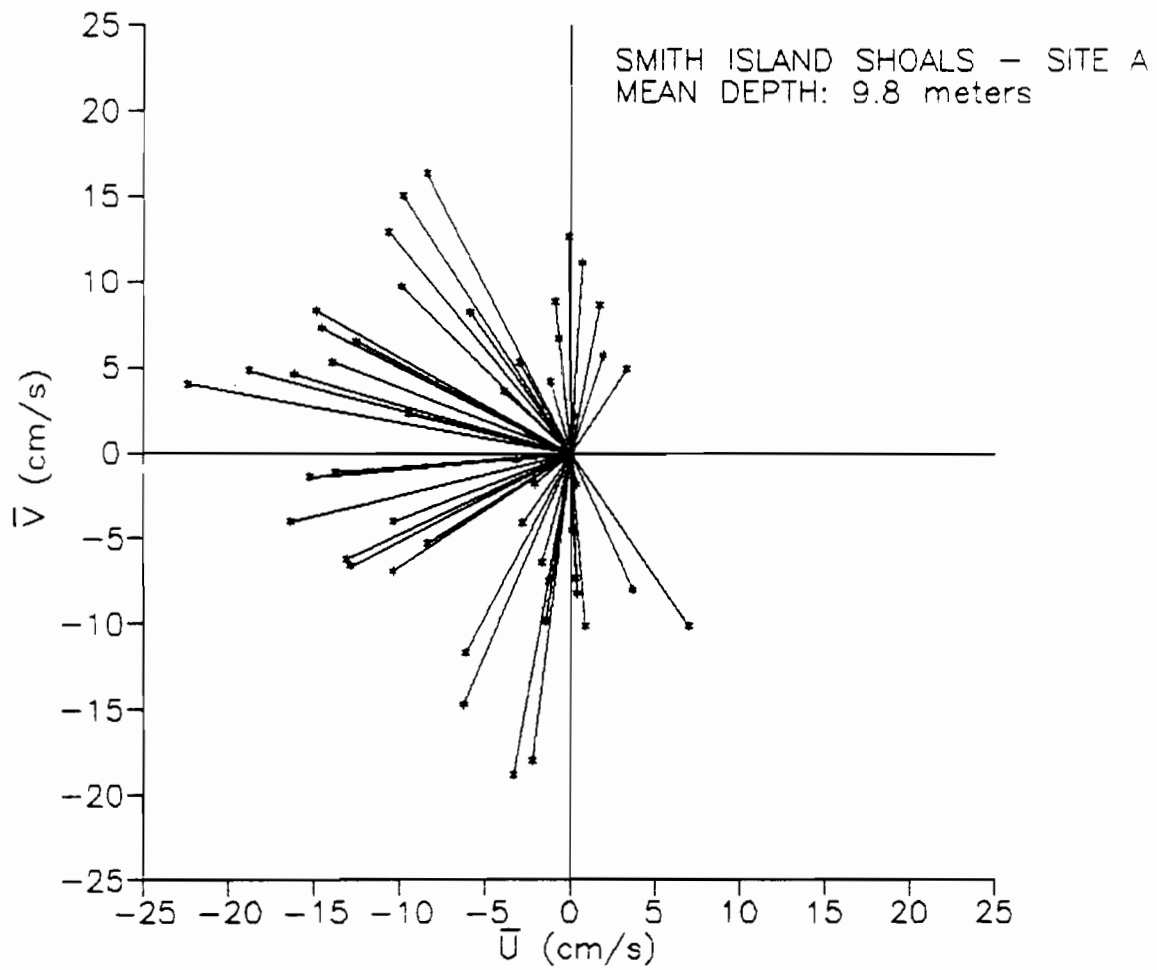


Figure 4. Vector diagram of hourly mean bottom current at site A for the 50-hour period from 0300 EST, 23 August 1987 to 0400 EST, 25 August 1987.

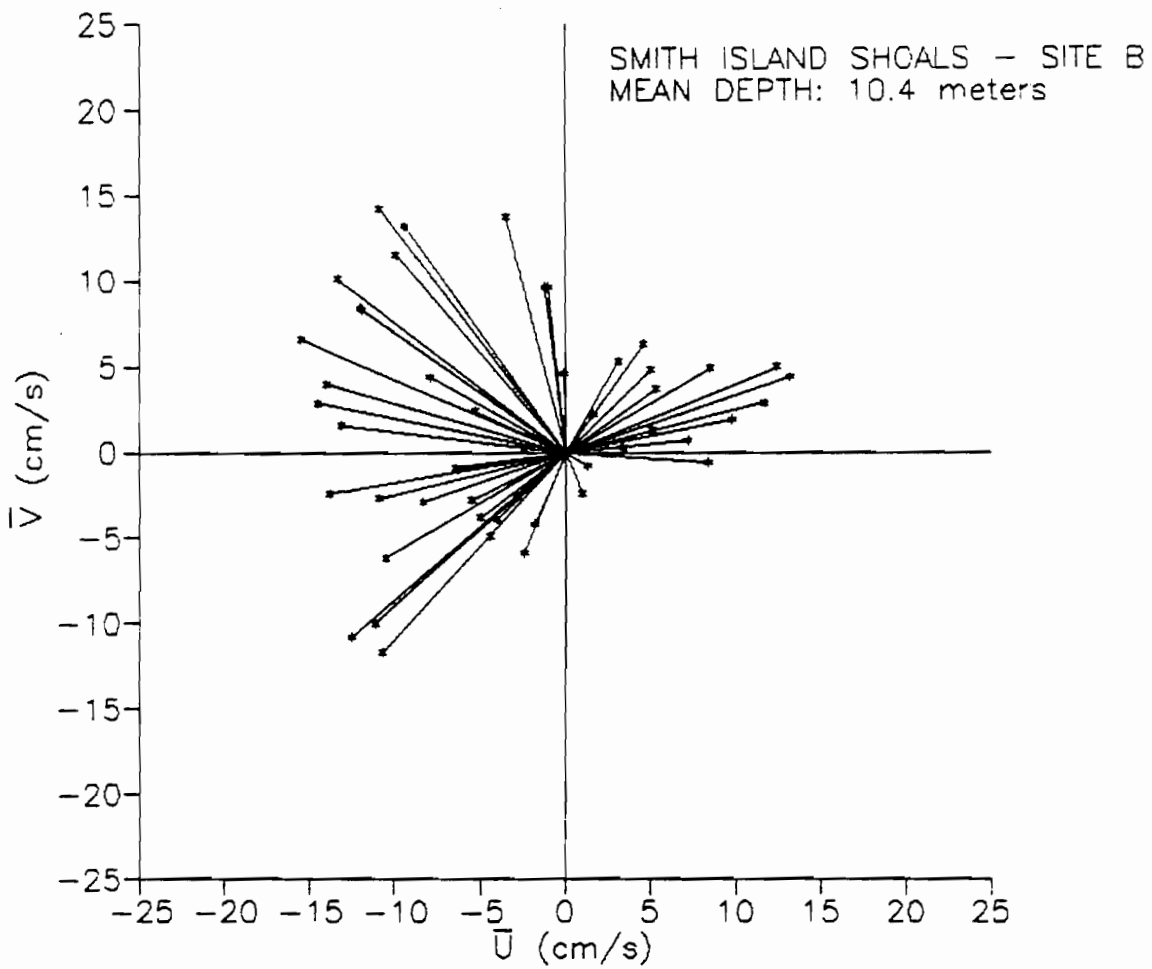


Figure 5. Vector diagram of hourly mean bottom current at site B for the 50-hour period from 0300 EST, 23 August 1987 to 0400 EST, 25 August 1987.

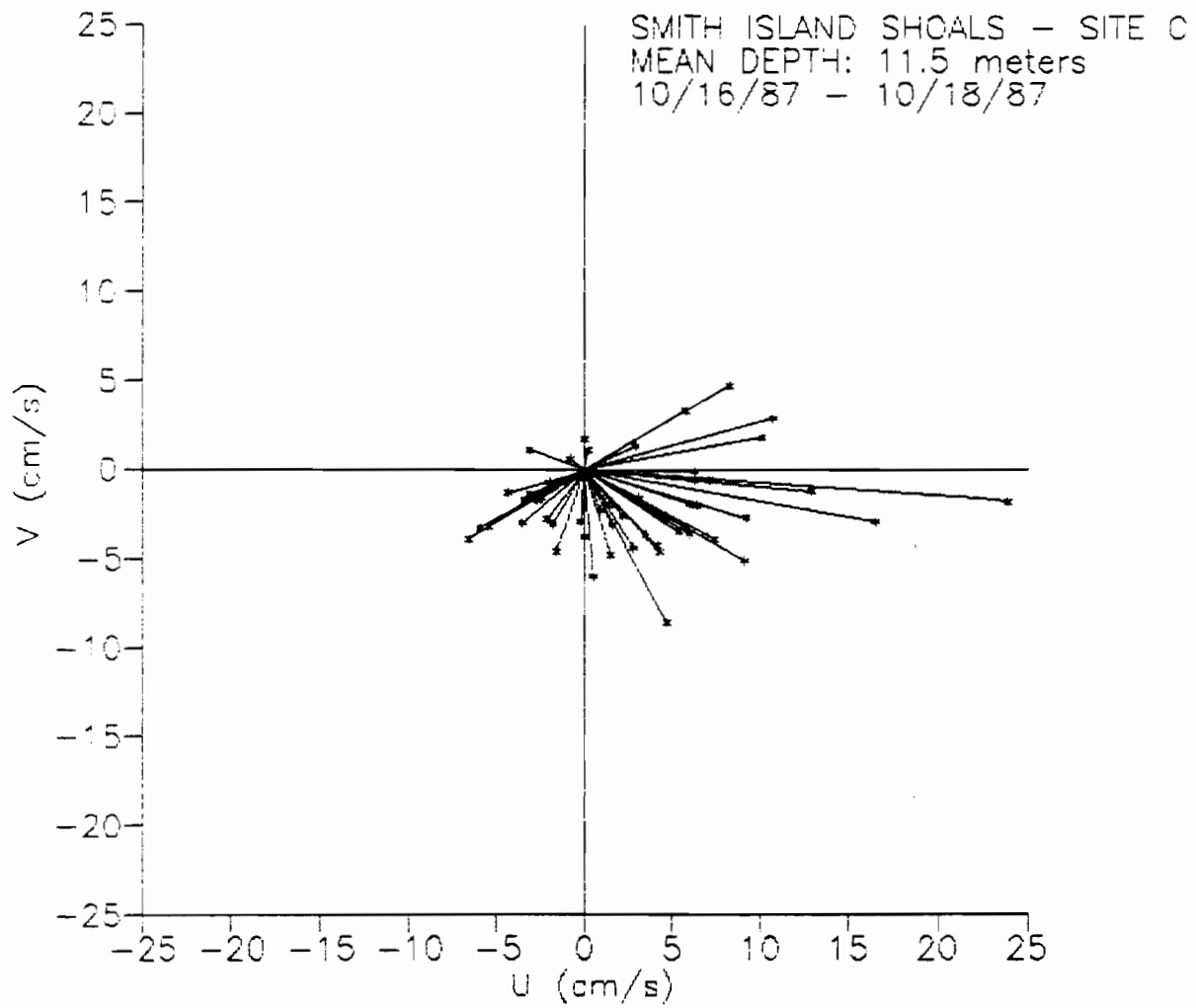


Figure 6. Vector diagram of hourly mean bottom current at site C for the 50-hour period from 0900 EST, 16 October, 1987 to 1100 EST, 18 October, 1987.

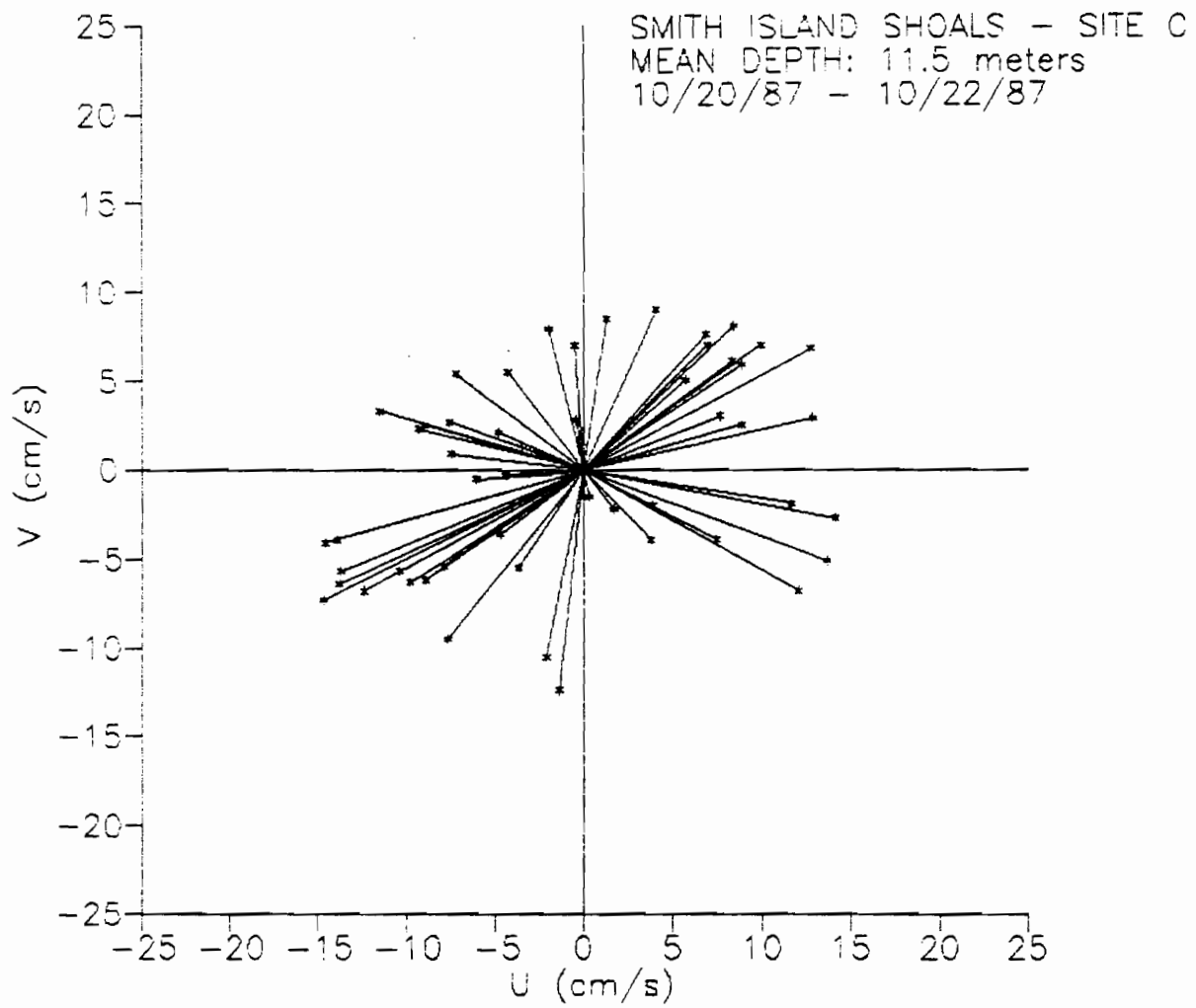


Figure 7. Vector diagram of hourly mean bottom current at site C for the 50-hour period from 0900 EST, 20 October, 1987 to 1100 EST, 22 October, 1987.

correlated with corresponding pressure (P) or corrected sea level (CSL) readings to resolve the 180-degree directional ambiguity based on the assumption of progressive wave motion.

Corrected sea level (CSL) readings were obtained using the fluctuating pressure series and a procedure developed by Nielsen (1986) which uses local frequency approximation rather than spectral methods for restoration of higher frequency oscillations attenuated with depth in accordance with linear wave theory. After reducing the CSL readings to their zero-mean values, the significant wave height ($H_{1/3}$) was computed as the equivalent of the zero-moment wave height (H_{m0}), following Goda (1974), using

$$H_{m0} = 4 \sigma \quad (1)$$

where σ is the standard deviation of the zero-mean CSL values over a burst. Using the same series, the average zero-up-crossing wave period, T , was calculated for each burst. These statistics, along with the burst-averaged total depth, are included at the bottom of each scattergram as shown in Figure 8.

Bottom Orbital Velocities

Of particular interest in this study is the maximum near-bottom velocity which, upon exceeding a critical value, will initiate sediment motion at the bed. By rotation of the U,V coordinate axes until the U+ axis aligns with either the mean flow direction or the modal wave direction (depending on which has the greater magnitude - wave orbital or mean flow), one obtains the maximum velocity for a given situation. For the present data, the maximum velocity resulted in all cases from alignment with the modal wave direction, as illustrated in Figure 8. Following the latter rotation, we obtained what will be termed the wave-current velocity component, U_{wc} , whose maxima are of primary interest with regard to sediment motion. Examples of a time series of U_{wc} are shown in Figure 9. Note that the wave velocity component, U_w , results after subtraction of the mean current component in the direction of wave motion (6.6 cm/s in Figure 9) from U_{wc} .

Initial Sediment Motion

The threshold of sediment motion under waves of increasing orbital velocity has been addressed by numerous authors. A review by Komar and Miller (1973) led to the following empirical equation predicting the Mobility Number, M , for grain diameters less than 0.5 mm (medium sand and finer):

$$M = \rho U_w^2 / (\rho_s - \rho) g D = 0.21 (2a/D)^{1/2} \quad (2)$$

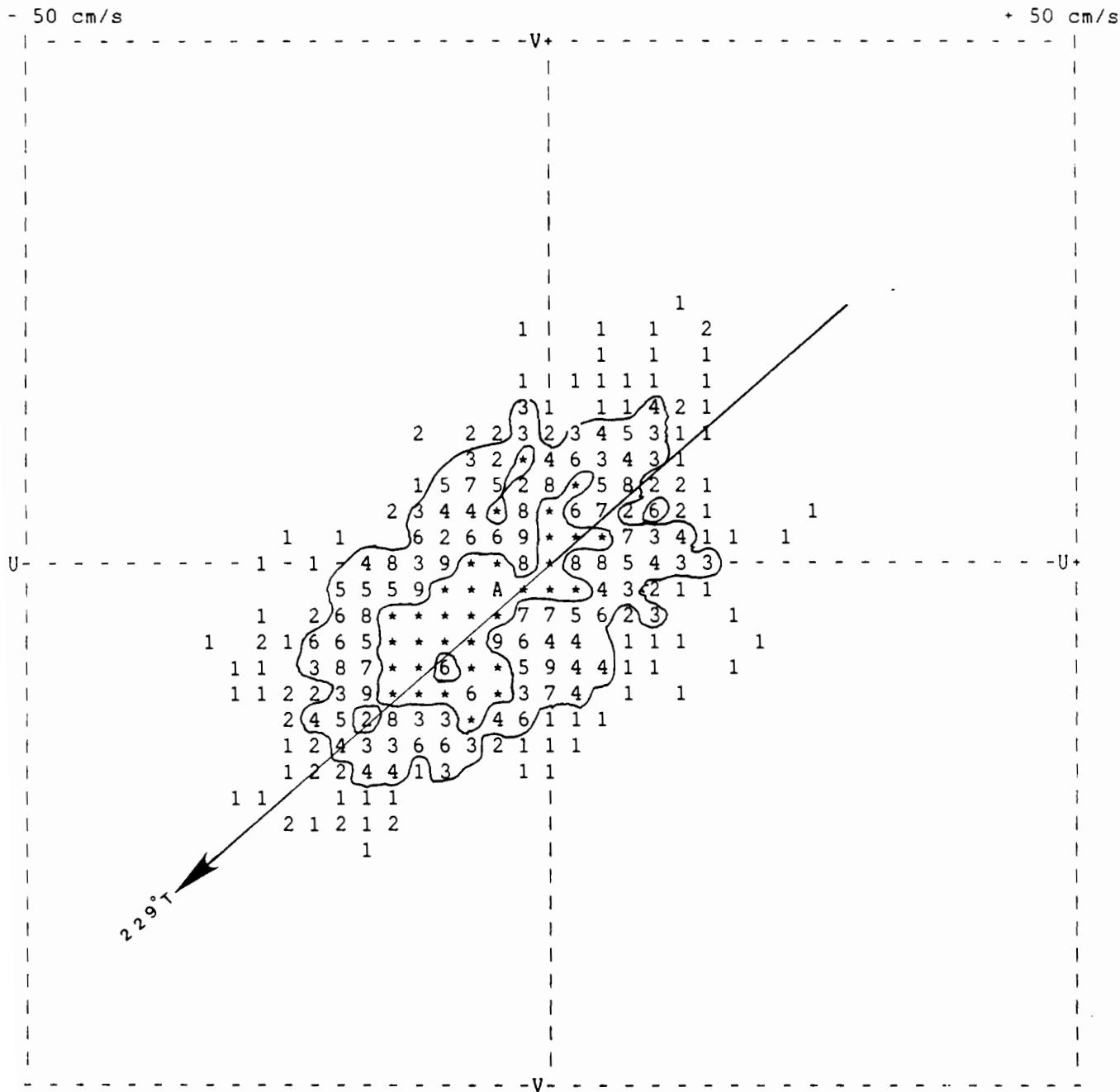
where ρ is the fluid density, ρ_s is the grain density, D is the grain diameter, g is the acceleration of gravity and a is the orbital amplitude of the wave motion defined by $a = U_w T/2$. Given a 10-second wave period, equation (2) predicts that a bed of quartz grains of 0.5 mm diameter should experience initial motion at a threshold orbital velocity of about 26 cm/s. However, more recent research has shown that initial motion will depend upon bottom roughness and the corresponding type of bottom flow (hydraulically rough or smooth). Initially plane beds that subsequently experience grain motion under waves will develop ripples which add significantly to bottom roughness. Beds that are already rippled during a time of increasing flows may therefore experience threshold grain motion at a much lower minimum orbital velocity.

Comparison of experimental data for initial motion in oscillatory flows with the well-known Shields curve for initial grain motion under steady flows (e.g., Sleath, 1984, p. 260) shows that a slightly more reasonable result than equation (2) may be obtained for very fine to medium sand using the threshold value of the Shields Entrainment Function:

$$\tau_o / (\rho_s - \rho) g D \sim 0.05 \quad (3)$$

where τ_o is the critical bottom shear stress for grain motion which in turn may be estimated using Jonsson's (1966) equation

$$\tau_o = 1/2 f_w \rho U_{wm}^2 \quad (4)$$



Ubar = -5.7 Vbar = -3.4 N = 1024 (1-1024) all points plotted onscale!
 Rbar = 6.7 Theta= 239.4
 Modal Wave_dir = 228.6 RV = 0.779 r(U^P) = -0.941
 TD= 10.96 m Hmo= 0.611 m T= 9.85 s

Figure 8. Scattergram of wave orbital velocities, 1300 EST 17 August 1987.

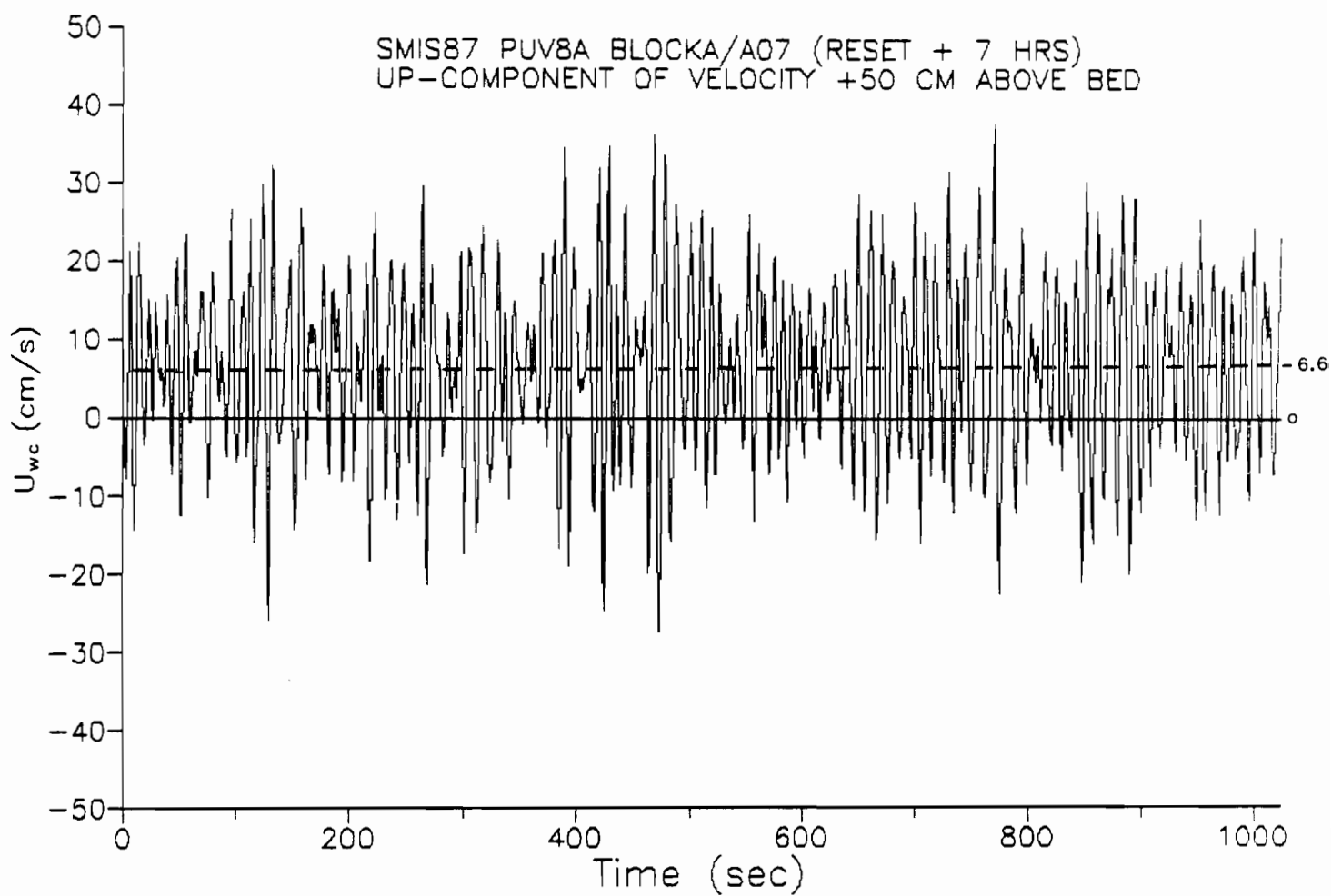


Figure 9. Combined wave and current in the direction of wave advance, 1300 EST, August 17, 1987, Site B.

in which U_{wm} is the maximum wave orbital velocity and f_w is the wave friction factor. Various means of obtaining f_w may be found but one that appears to show good agreement with a wide range of experimental data is Kajiura's (1968) equation

$$f_w = 0.35 (a/k_s)^{-2.3} \quad (5)$$

wherein k_s is a roughness length given by Swart (1976) as

$$k_s = 25 h^2/L \quad (6)$$

and h and L are the ripple height and wave length, respectively. Other equations presented by other researchers predict somewhat different values of k_s as a function of h/L , pointing out the variability inherent in this parameter.

Equations (3) - (6) outline one example of the wave friction approach for estimating the amplitude of the orbital velocity needed to initiate grain motion. The predicted velocities are probably conservative in that the additional factor of wave-current interaction (Grant and Madsen, 1979), which tends to increase the stress experienced at the bed above that predicted for combined waves and currents without interaction, has not been considered. There are instances in our deployments when both waves and steady currents are clearly important (Figure 9).

Given the various conditions which determine f_w , the wave friction factor, it is clear that a range of threshold velocities are possible. For a flat bed of coarse sand and wave conditions such as those indicated in Figure 8, a wave friction factor of $f_w = 0.006$ should result (Sleath, 1984, p.196) but this value may increase several-fold to approximately $f_w = 0.1$ as bedforms are encountered of the type previously described at sites A and B, according to equations (5) and (6). Figure 10 shows the range of orbital velocities likely to be required to initiate motion given the grain sizes, grain densities and wave friction factors considered possible at these sites.

INTERPRETATION OF RESULTS

Sediment Motion Induced by Waves

The measurement data for the first deployment (sites A and B) provide an example of what may be termed "fairweather" conditions. The entire deployment took place during a period of moderating wind and wave activity following a storm that had occurred the week before. Nevertheless, the swell which continued to arrive at sites A and B during the first two to three days of the experiment maintained a significant wave height of between 0.4 and 0.6 meters with a wave period of between 9 and 10 seconds. These waves continued to produce approximately the same level of bottom orbital motion as illustrated in Figure 9 wherein peak orbital velocities frequently exceed 20 cm/s and occasionally exceed 30 cm/s. Very little, if any, difference was noted in the peak velocity values observed at site B (ridge flank) and site A (ridge crest), probably due to their close proximity and slight difference in mean water depth.

The measurement data for the second deployment (site C) in October 1987 provide an example of moderate energy conditions (significant wave heights of 0.8 to 1.0 meter, 8.5 to 9.5 second wave periods) with much greater wave-current velocities at 50 cm above the bed as compared to the August 1987 measurements. As shown in Figure 11, U_{wc} values reached a maximum of slightly more than 80 cm/s in combination with a U_c value averaging about 23 cm/s during the early phases of the deployment.

If the sand ripple dimensions initially observed by our divers during the first deployment are representative (some signs of bed smoothing were noted by the end of the experiment), it is likely that a fairly high value of the wave friction factor may apply (roughly $0.07 < f_w < 0.1$) much of the time at sites B and C. Assuming this is the case, Figure 10 then predicts that even the heaviest minerals in the fine sand fraction will experience initial motion assuming a critical orbital velocity of 10 cm/s or more. Our data indicate that velocities of more than twice this value will be experienced under normal fairweather conditions. Vigorous sediment motion (well beyond incipient grain movement) is indicated for the moderately energetic conditions experienced during the early phases of the second deployment. High energy conditions prevail during passage of extratropical lows in winter, spring and fall at which time the actual deployment or recovery of a tripod from our 60-foot research vessel becomes impossible to carry out.

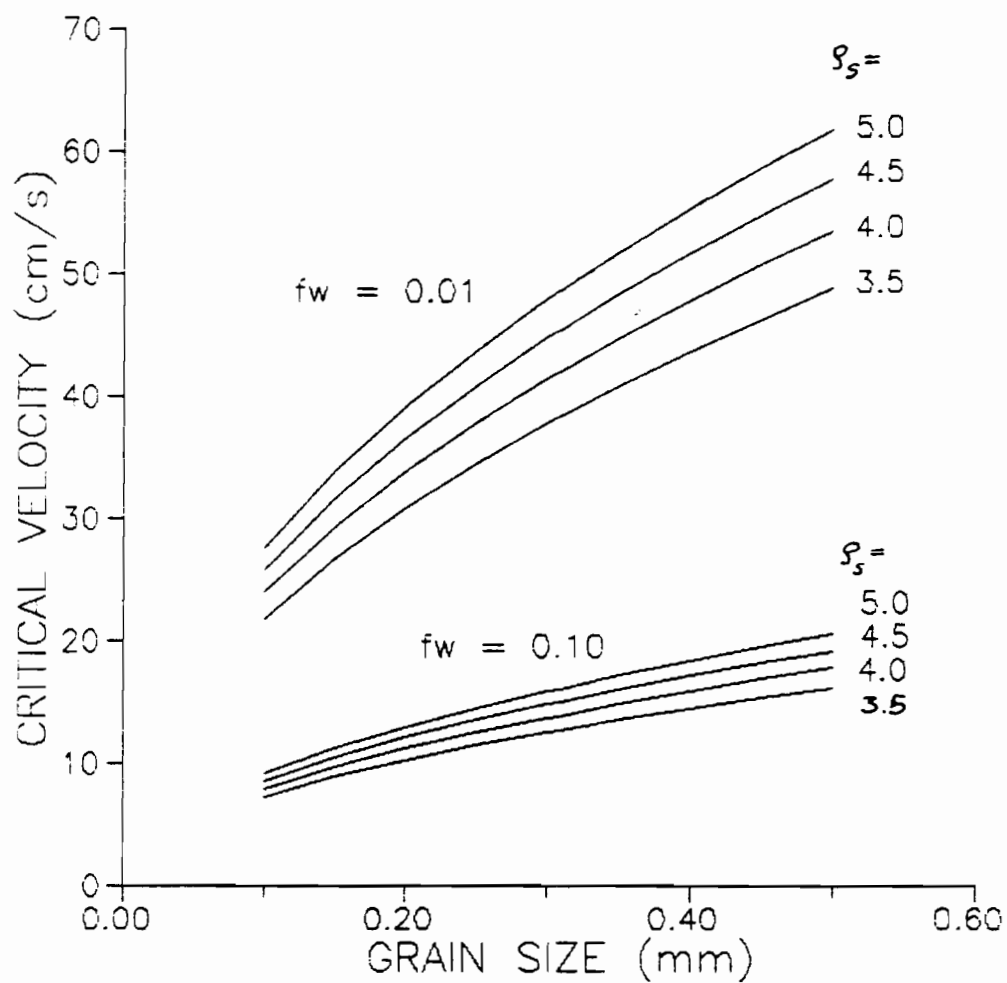


Figure 10. Critical velocity for initial grain motion in oscillatory flow based on equations (3)-(6).

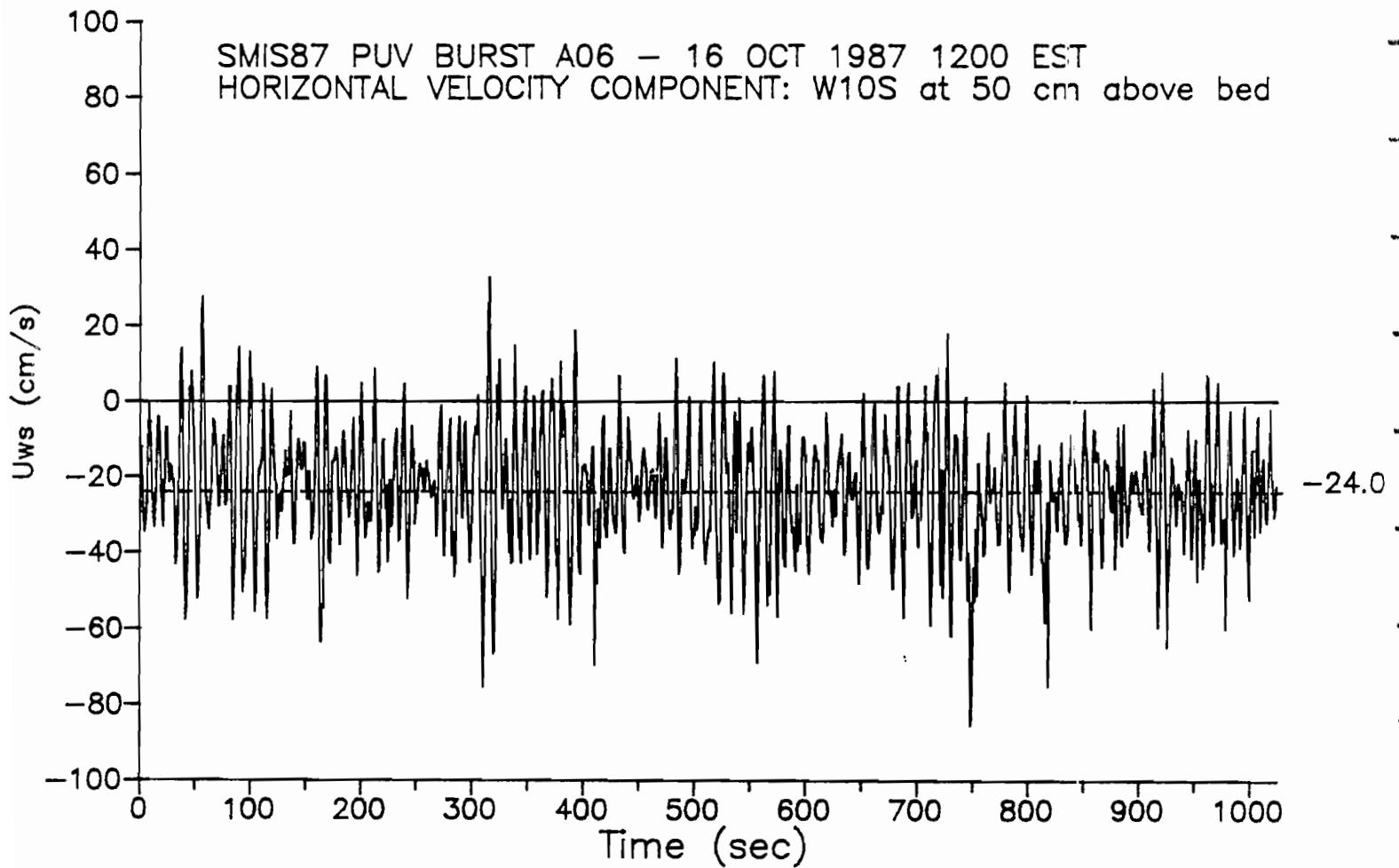


Figure 11. Combined wave and current in the direction of wave advance, 1200 EST, 16 October 1987, Site C.

From the above evidence, our general conclusion is that the bottom region of Smith Island Shoal is indeed shoal to the point where sediment entrainment by waves, certainly those with periods longer than 9 seconds, is rather commonplace and not at all limited to periods of intense storm activity. The following observations of the suspended sediment field near the bottom also suggest that local entrainment, settling and resuspension of bottom sediment are active processes occurring during moderate wave energy conditions.

Sediment Resuspension Layer

Temporal variations in suspended sediment concentration at a fixed point near the sea bed can occur in either of two ways: 1) in response to the vertical flux of material being eroded from or deposited on the bed locally, or 2) in response to horizontal advection of turbid (or clear) water from another area. A time series of measurements from a single point ordinarily does not offer sufficient means to resolve the two. However, variation at a time scale matching that of the wave motion is evidence of vertical flux and a vertical array of sensors can be used to demonstrate bed layer resuspension under these conditions.

Concentration of suspended sediment was successfully monitored by the OBS array during the second deployment. Figure 12 contains a sample burst depicting 8-second averages of suspended sediment concentration measured at five different elevations above the bed. These span the same time interval as the current field shown in Figure 11 and a comparison of the latter with the output of the lower four OBS sensors in Figure 12 indicates positive coherence at roughly the same phase.

Strong flow peaks associated with wave group maxima match peaks in concentration reasonably well. However, the fifth OBS sensor output shown in Figure 12 reveals relatively little variation about a burst mean of approximately 450 mg/l at the 1 meter elevation above the bed. The progressive and rapid increase in concentration variance below this level of marginal change suggests the presence of a layer of active resuspension involving bed material. Suspended sediment concentrations vary between 1 and 2 g/l within 10 cm of the bed at a time scale of roughly 100 to 200 seconds matching the groupiness period of the waves.

Additional evidence of the resuspension process can be seen in Figure 13. This figure contains profile lines of best fit to log elevation versus log concentration data derived from 32-second averages of the OBS signals at each of the five measurement elevations. A typical time-consecutive sequence of four lines, each fitting their 5 data points reasonably well (r^2 values of 0.95 to 0.98) begin a phased resuspension event by showing an initial concentration increase at the bed (lines 1 to 2, increasing slope phase) followed by a rise of the material upward (lines 3 and 4, decreasing slope phase) within an approximate half-cycle period of 128 seconds.

Potential Sediment Transport due to Currents

Mean currents measured near the bed were not of high strength, as we believed they might be because of the proximity of Smith Island Shoal to the Chesapeake Bay entrance. We found that non-spring steady flows only occasionally exceeded 10 cm/s at Smith Island Shoal which is typical of tidal currents on the inner shelf areas of the Middle Atlantic Bight away from estuarine entrances (Beardsley and Boicourt, 1981). Flood and ebb surface currents are highest on the northern side of the Chesapeake Bay entrance between Fishermans Island and Cape Charles where near-bottom and surface flows average approximately 100 cm/s (Browne and Fisher, 1988).

Plots of the hourly mean current vectors which we obtained near the peak flow of a spring tide (Figures 4 and 5) show a clockwise rotation pattern somewhat indicative of rotary tidal currents; however, they do not include the typical "elliptic" pattern featuring major and minor flow axes arranged more or less at right angles to one another. Figures 4 through 7 suggest either that the topography associated with the ridge exerts a "steering" influence on the bottom flow, favoring certain flow directions, or else transient (wind-induced) streams may augment the bottom tidal flows in this region. While the mean flow may not be sufficiently high to effect sediment entrainment much of the time, it will undoubtedly influence transport pathways for sediment placed in suspension by waves.

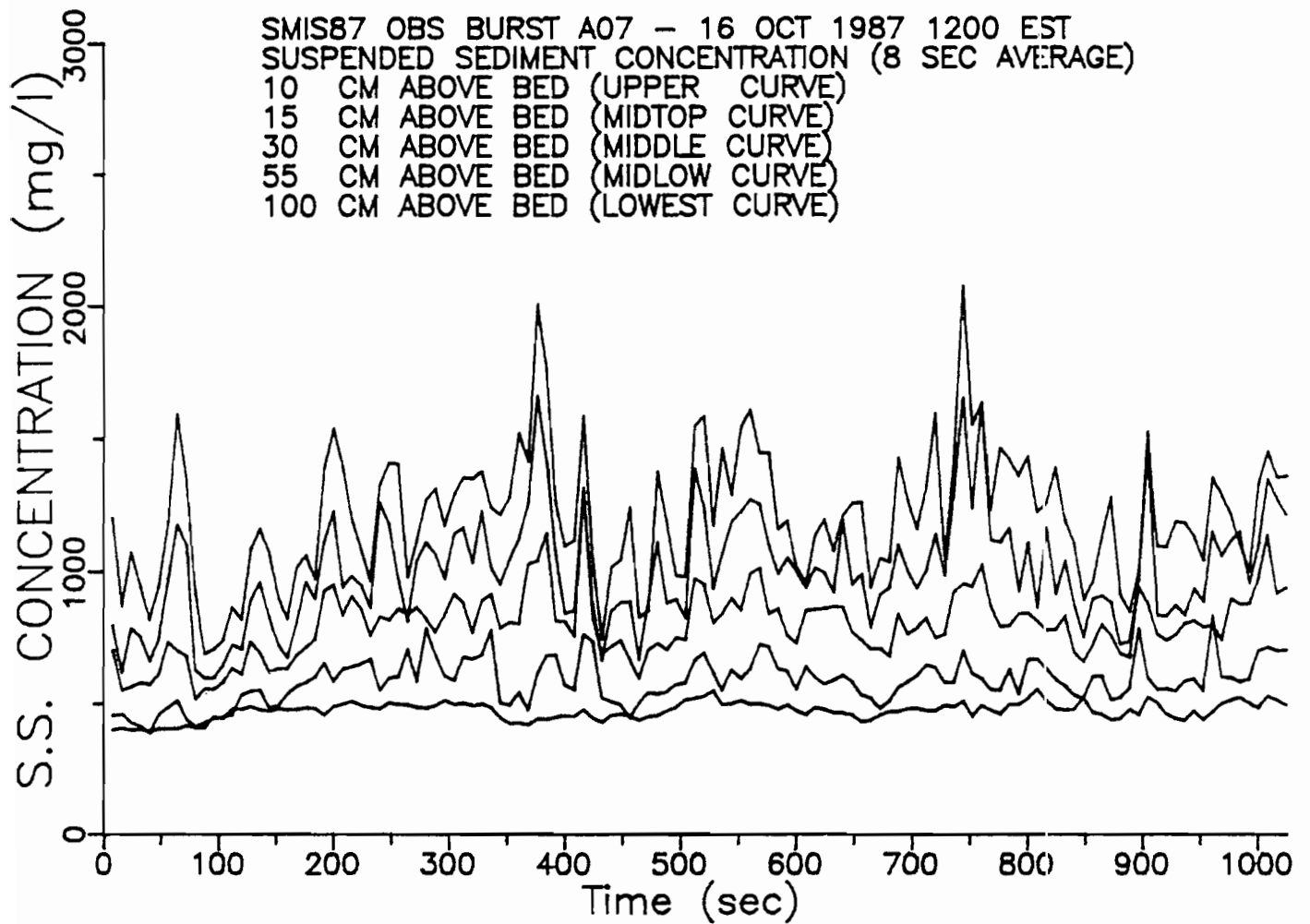


Figure 12. Plot of suspended sediment concentration at 5 elevations above the bed, 1200 EST, 16 October 1987, Site C.

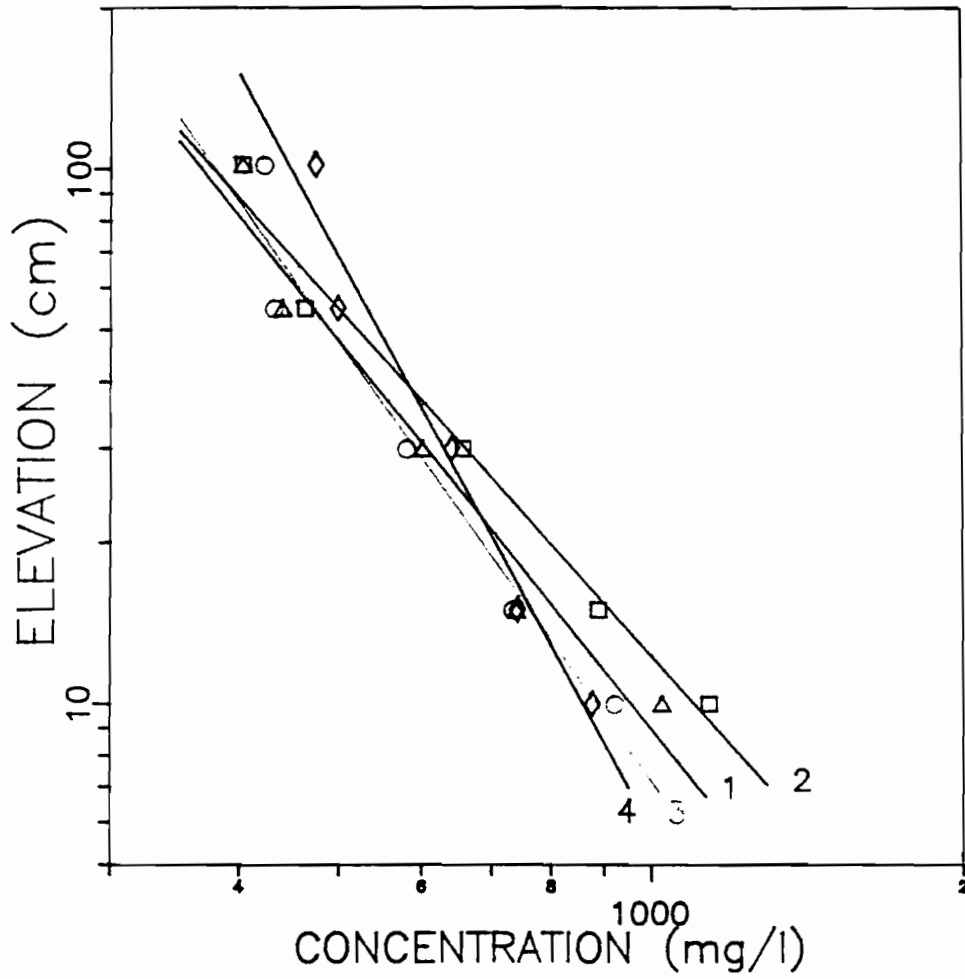


Figure 13. Profiles of suspended sediment concentration averaged successively over 32-second intervals.

Heavy Mineral Enrichment

Only a few studies have examined the question of how heavy mineral enrichment may occur in the marine environment other than on beaches. In one of them, Barrie (1981) proposed a model of enrichment based on the hydraulic inequivalence of heavy and light mineral fractions observed in the Bristol Channel, England. In addition to grain size limitations associated with the original source of heavy minerals, Barrie cited differential entrainment as a mechanism for producing hydraulic inequivalence (grains larger or smaller than expected) among grains of different density found in the same deposit. According to Slingerland (1977), hydraulic inequivalence associated with hydrodynamically rough flows and a coarse, poorly sorted deposit, may produce heavy minerals with grain diameters up to four times smaller than predicted from standard hydraulic equivalence. These smaller-sized "heavies" will then lodge within the larger population resulting in a general increase in the percentage of heavy minerals since larger/lighter grains with the same hydraulic equivalence will have been removed by fluid turbulence.

We find Barrie (and Slingerland's suggestions interesting, noting that Figure 9 implies that grains of different density but similar size respond to a wider range of critical entrainment velocities when the wave friction is low. However, Barrie observed that the greatest heavy mineral enrichment occurred in areas of high tidal current intensity that were also well sheltered from wave oscillatory flow. In these regions, he called upon a "lag" hypothesis to explain enrichment wherein lighter grains simply roll away with the unidirectional current, leaving the heavier grains behind.

Based on our field observations to date, high intensity tidal flows combined with low oscillatory flows are virtually the opposite of conditions prevailing at Smith Island Shoal. While tidal currents are not expected to be much larger than those already observed, it is virtually certain that much larger wave oscillatory flows occur during storm periods. Orbital velocities in excess of 90 cm/s have been observed near the sea bed off Dam Neck, Virginia, during winter storms (Boon and others, 1987).

A specific mechanism satisfactorily explaining hydraulic enrichment of heavy minerals in association with sand ridge features is not apparent at this time and none has been suggested from the data collected thus far. We believe, however, that entrainment processes should receive further attention, particularly with regard to bottom stress and hydraulic equivalence or inequivalence among grains of different density. To that end, it will also be important to determine which minerals are being entrained and the relative abundances of heavy versus light minerals in the water column.

Heavy Minerals Found in Suspension

Tables are included in Appendix B summarizing the mineral composition of the suspended material trapped just above the bed (at heights of 25, 40, 60, 80 and 150 cm) during the first (August 1987) and second (October 1987) deployments.

The composition of suspended sediment does not differ greatly from either surficial grab samples or samples of the upper sections of cores taken in the tripod deployment area (Table 1). In agreement with the suspended sediment evidence noted above, the mineralogy of the trapped material suggests that it is locally derived. "Pyroboles" are the most common minerals throughout the study area. Ilmenite, garnet, and epidote are the next most common minerals in suspended sediment and in cores.

There is one aberration among the common mineral compositions. Zircon is the second most abundant mineral but in grab samples only. The lack of zircon in suspended sediment might be explained by zircon's high specific gravity (4.6 to 4.7) and low overall abundance (cores). However, ilmenite also has a high specific gravity (approximately 4.7) and is commonly found in suspension. These observations have two possible explanations. Firstly, preferential entrainment of ilmenite amid lagging of zircon may have occurred at the sediment-water interface. Secondly, there may be more ilmenite in the water column because there is relatively more of this mineral in the surficial sediments locally or in transit from other areas. However, the second explanation is not supported by our grab sample data and the strong evidence for active local resuspension. Differential entrainment may be indicated indirectly by greater heavy mineral concentrations observed at the sediment surface (in grab samples) rather than below the surface layer (in cores).

Table 1. Comparison of average composition of sediment from different environments at the Smith Island Shoal. "Pyrobole" is the sum of pyroxene and amphibole abundance.

Suspended sediment (This report)	Cores (Upper Section) (Berquist and Hobbs, 1988)	Grab Samples (Berquist and Hobbs, 1986)
"pyrobole"	"pyrobole"	"pyrobole"
ilmenite	ilmenite	zircon
epidote	garnet	ilmenite
garnet	epidote	epidote-garnet

REFERENCES CITED

- Beardsley, R.C., and W.C. Boicourt, 1981, On estuarine and continental circulation in the Middle Atlantic Bight, *in* B.A. Warren and C. Wunch (editors), *Evolution of Physical Oceanography*, MIT Press, Cambridge, MA, p. 198-233.
- Berquist, C.R., Jr., and C.H. Hobbs, 1986, Assessment of economic heavy minerals of the Virginia Inner Continental Shelf: Virginia Division of Mineral Resources Open-file Report 86-1., 17 p.
- Berquist, C.R., Jr., and C.H. Hobbs, 1988, Study of economic heavy minerals of the Virginia Inner Continental Shelf: Virginia Division of Mineral Resources Open-file Report 88-4., 149 p.
- Boon, J.D., W. Frank Bohlen, and L.D. Wright, 1987, Estuarine versus inner shelf disposal sites: A comparison of benthic current regimes. *Coastal Sediments 87*, ASCE, New Orleans, May 1987, p. 571-583.
- Browne, D.R., and C.W. Fisher, 1988, Tides and tidal currents in the Chesapeake Bay: NOAA Technical Report NOS OMA 3, U.S. Department of Commerce, Rockville, MD, 84 p. and appendices.
- Goda, Y., 1974, Estimation of wave statistics from spectral information: Proceedings of the International Symposium on Ocean Wave Measurement and Analysis, New Orleans, LA, Sept. 1974, p. 320-337.
- Grant, W.D., and O.S. Madsen, 1979, Combined wave and current interaction with a rough bottom: *Journal Geophysical Research*, v. 84, p. 1779-1808.
- Jonsson, I.G., 1966, Wave boundary layers and friction factors: Proceedings of the 10th International Conference on Coastal Engineering, Tokyo, ASCE, p. 127-148.
- Kajiura, K., 1968, a model of the bottom boundary layer in water waves: *Bulletin Earthquake Research Institute*, v. 46, p. 75-123.
- Komar, P.D., and M.C. Miller, 1973, The threshold of sediment movement under oscillatory water waves: *Journal Sedimentary Petrology*, v. 43, p. 1101-1110.
- Nielsen, P., 1976, Local approximations: a new way of dealing with irregular waves: Proceedings of the 20th International Conference on Coastal Engineering, Taiwan, ASCE.
- Sleath, J.F.A., 1984, *Sea Bed Mechanics*. John Wiley & Sons, New York, 335 p.

Slingerland, R.L., 1977, The effects of entrainment on the hydraulic equivalence relationships of light and heavy minerals in sands: *Journal Sedimentary Petrology*, v. 47, p. 753-770.

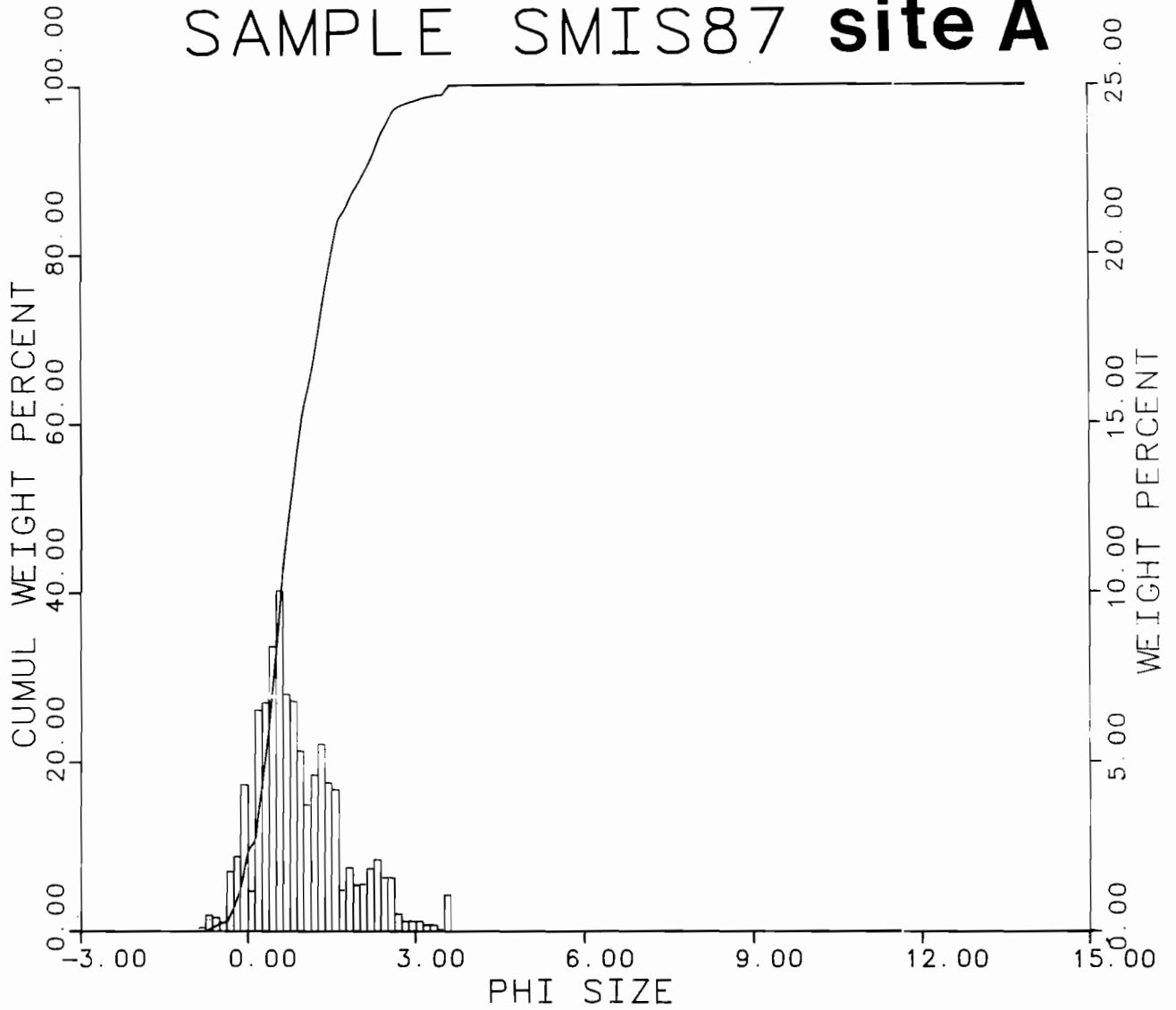
Stubblefield, W.L., J.W. Lavelle, T.F. McKinney, and D.J.P. Swift, 1975, Sediment response to the present hydraulic regime on the Central New Jersey shelf: *Journal Sedimentary Petrology*, v. 45, p. 337-358.

Swart, D.H., 1976, Coastal sediment transport: Computation of longshore transport: Delft Hydraulics Laboratory Report, R968, Part 1.

Swift, D.J.P., 1976, Coastal Sedimentation, *in* Stanley, D. J., and Swift, D. J. P., editors, *Marine Sediment Transport and Environmental Management*, John Wiley & Sons, p. 255-310.

APPENDIX A: BOTTOM SEDIMENT GRAIN SIZE ANALYSES

SAMPLE SMIS87 site A



Sample Location

LATITUDE ——— 0-0-0
 LONGITUDE ——— 0-0-0
 DEPTH (m) ——— 0.00

Gross Parameters

GRAVEL (%) ——— 2.6
 SAND (%) ——— 80.8
 COARSE SAND (%) — 52.2
 MEDIUM SAND (%) — 26.9
 FINE SAND (%) — 9.6
 V-FINE SAND (%) — 1.8
 SILT (%) ——— 2.1
 CLAY (%) ——— 14.5

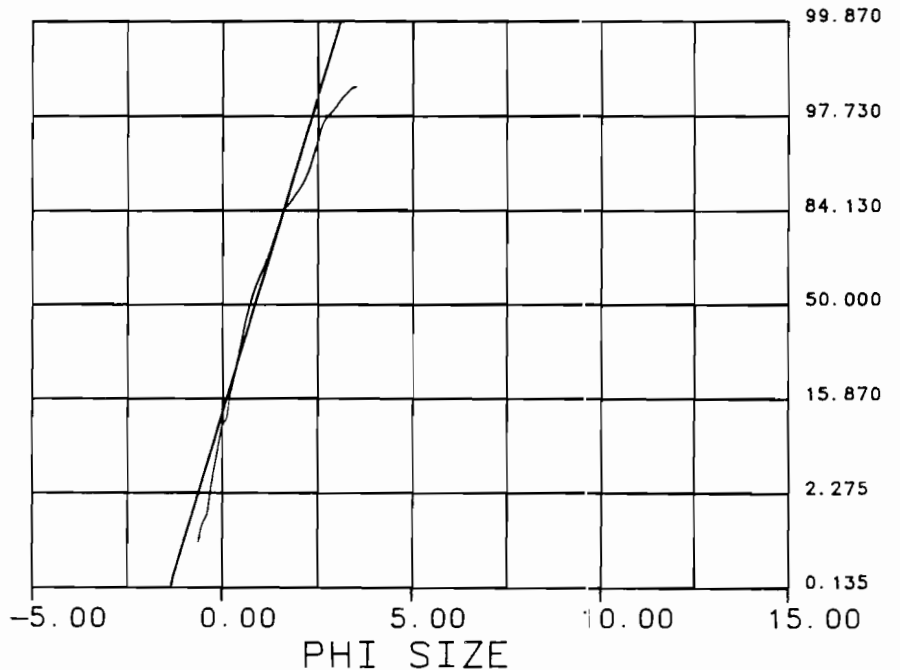
Graphic Measures

MODE ——— 0.758
 MEAN ——— 0.868
 STD. DEVIATION — 0.741
 INC. SKEWNESS — 0.273
 INC. KURTOSIS — 0.884

Moment Measures

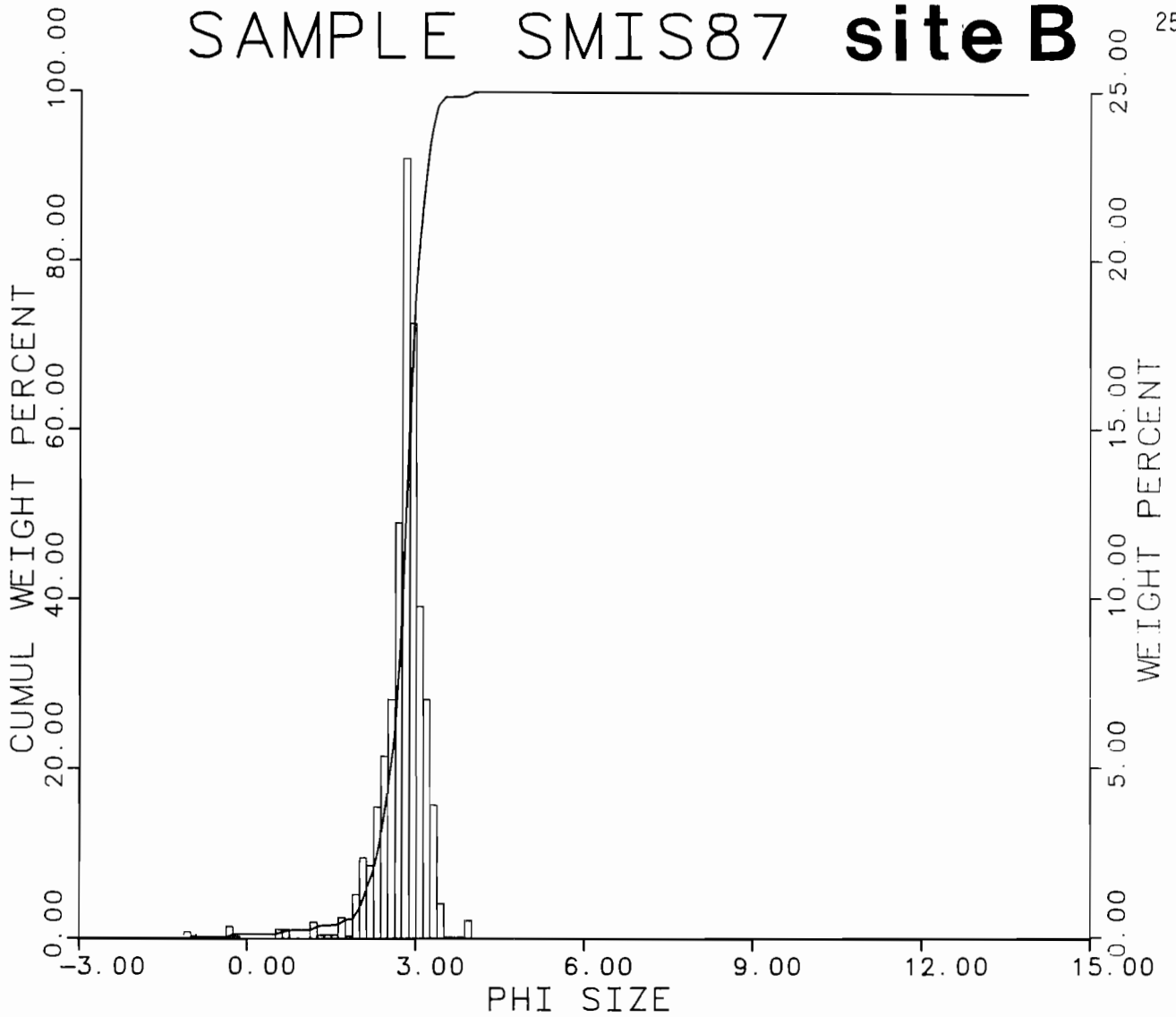
1st MOMENT ——— 0.926
 2nd MOMENT ——— 0.791
 3rd MOMENT ——— 0.859
 4th MOMENT ——— 3.715

PROBABILITY CURVE



OBSERVED SIZE DISTRIBUTION
 GAUSSIAN PROBABILITY Based on Graphic Mean and Std. Dev

SAMPLE SMIS87 site B



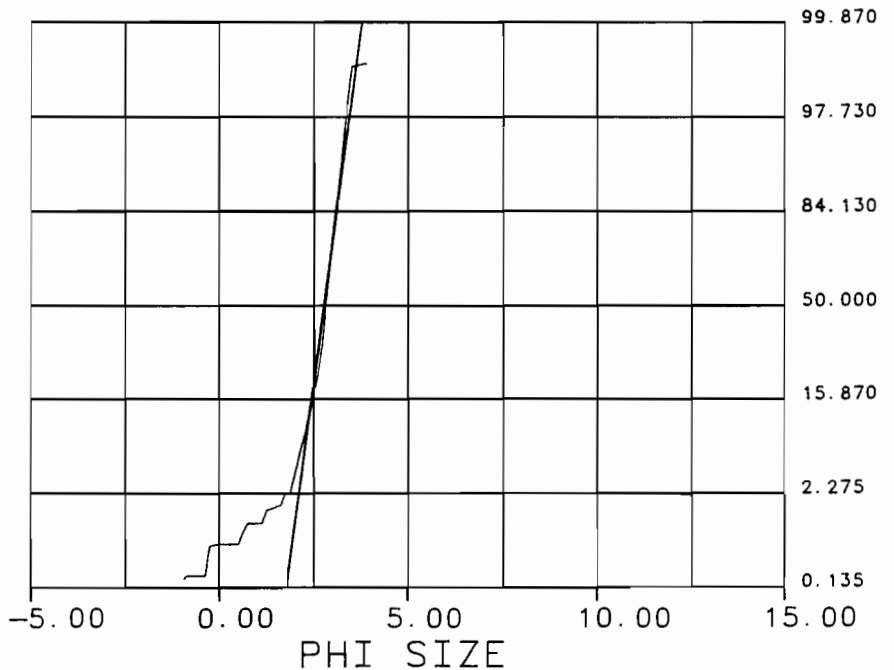
Sample Location
 LATITUDE ——— 0-0-0
 LONGITUDE ——— 0-0-0
 DEPTH (m) ——— 0.00

Gross Parameters
 GRAVEL (%) ——— 0.1
 SAND (%) ——— 80.2
 COARSE SAND (%) — 0.5
 MEDIUM SAND (%) — 2.6
 FINE SAND (%) — 74.1
 V-FINE SAND (%) — 22.3
 SILT (%) ——— 1.7
 CLAY (%) ——— 18.0

Graphic Measures
 MODE ——— 2.823
 MEAN ——— 2.791
 STD. DEVIATION — 0.333
 INC. SKEWNESS — -0.207
 INC. KURTOSIS — 0.257

Moment Measures
 1st MOMENT ——— 2.757
 2nd MOMENT ——— 0.449
 3rd MOMENT ——— -3.128
 4th MOMENT ——— 22.140

PROBABILITY CURVE



OBSERVED SIZE DISTRIBUTION
 GAUSSIAN PROBABILITY Based on Graphic Mean and Std. Dev

APPENDIX B: SUSPENDED SEDIMENT MINERAL COMPOSITION

MINERAL	SAMPLES FROM FIRST DEPLOYMENT (AUGUST 1987)					AVERAGE (both deployments)
	25CM	40CM	60CM	90CM	150CM	
RUTILE	2.1	2.3	1.3	1.8	2.4	1.9
HI-Ti(85-99%) LEUCOXENE	1.2	0.8	1.3	0.9	2.3	1.0
LO-Ti(65-85%) LEUCOXENE	1.6	0.4	1.7	0.4	1.4	1.1
PRIMARY(57-65%)ILMENITE	4.5	4.7	3.3	4.8	0.5	3.1
SECONDRY(<57%) ILMENITE	7.7	3.8	6.1	6.3	2.6	5.2
Ti-MAGNETITE (<5%TiO2)	1.0	0.9	1.0	1.6	1.1	0.6
FE-OXIDE	1.0	2.4	2.1	3.7	0.6	1.7
QUARTZ	3.9	10.7	16.7	21.6	24.3	11.9
ZIRCON	1.8	2.5	0.9	0.5	0.0	1.1
MONAZITE	0.0	0.0	0.0	0.0	0.0	0.0
ALUMINO-SILICATE	0.6	1.4	0.6	0.0	0.0	0.7
APATITE	2.5	1.2	1.3	0.7	1.4	2.4
CHLORITE	0.3	1.3	0.7	0.0	0.0	0.5
BIOTITE	0.0	0.3	0.6	0.3	1.0	0.4
MUSCOVITE	0.3	2.1	2.0	1.5	1.3	1.7
GARNET	4.9	3.0	2.1	2.6	2.3	4.5
EPIDOTE	8.2	3.7	5.4	4.5	3.0	6.0
SPHENE	1.6	0.9	0.7	1.4	2.2	2.0
STAUROLITE	0.4	2.7	0.7	0.4	0.0	0.8
TOURMALINE	0.6	0.8	0.3	1.3	0.0	1.0
AMPHIBOLE AND PYROXENE	52.7	46.6	38.7	27.3	23.2	42.2
XENOTIME	0.0	0.0	0.0	0.0	0.0	0.1
K-FELDSPAR	0.3	0.7	2.6	2.1	2.6	1.2
PLAGIOCLASE	1.3	2.2	4.9	9.7	19.0	4.8
CALCITE	0.0	0.2	0.0	0.0	2.1	0.3
DOLOMITE	1.6	4.3	5.0	6.7	6.8	3.9
SUM	100.1	99.9	100.0	100.1	100.1	100.0

SUMMARY OF MINERAL COMPOSITIONS FROM CARPCO FEB 1989
SAMPLE COMPOSITION IN WT %

MINERAL	SAMPLES FROM SECOND DEPLOYMENT				
	#25	#40	#60	#80	#150
RUTILE	2.2	2.0	1.8	2.1	1.2
HI-Ti(85-99%) LEUCOXENE	0.4	1.2	0.0	1.2	0.8
LO-Ti(65-85%) LEUCOXENE	1.3	0.8	0.9	2.1	0.8
PRIMARY(57-65%)ILMENITE	1.9	3.1	2.4	2.8	3.5
SECONDRY(<57%) ILMENITE	4.3	5.8	1.9	4.6	8.8
Ti-MAGNETITE (<5%TiO ₂)	0.0	0.0	0.0	0.0	0.0
FE-OXIDE	0.0	1.5	1.1	1.5	2.9
QUARTZ	12.4	1.5	14.5	10.7	3.0
ZIRCON	0.9	0.4	1.4	0.0	2.2
MONAZITE	0.0	0.0	0.0	0.0	0.0
ALUMINO-SILICATE	1.0	0.3	0.7	1.3	0.6
APATITE	2.3	3.3	2.3	3.5	5.7
CHLORITE	1.8	0.6	0.3	0.3	0.0
BIOTITE	1.9	0.0	0.0	0.3	0.0
MUSCOVITE	5.3	0.8	2.4	1.4	0.0
GARNET	3.4	4.0	5.2	8.7	8.7
EPIDOTE	4.5	7.8	6.3	7.7	8.9
SPHENE	2.4	1.6	3.9	2.0	2.9
STAUROLITE	0.4	1.4	0.4	0.4	0.7
TOURMALINE	1.6	2.1	0.0	1.5	1.5
AMPHIBOLE AND PYROXENE	41.6	60.5	48.0	39.2	44.5
XENOTIME	0.5	0.0	0.0	0.0	0.0
K-FELDSPAR	0.8	0.2	1.1	0.8	1.0
PLAGIOCLASE	4.7	0.3	2.2	3.2	0.8
CALCITE	0.3	0.0	0.0	0.0	0.0
DOLOMITE	4.2	0.7	3.2	4.7	1.6
SUM	100.1	99.9	100.0	100.0	100.1

NORMALIZED COMPOSITIONS (LIGHT MINERALS REMOVED)

	SECOND DEPLOYMENT				
	#25	#40	#60	#80	#150
RUTILE	2.8%	2.1%	2.3%	2.6%	1.3%
HI-Ti(85-99%) LEUCOXENE	0.5%	1.2%	0.0%	1.5%	0.9%
LO-Ti(65-85%) LEUCOXENE	1.7%	0.8%	1.1%	2.6%	0.9%
PRIMARY(57-65%) ILMENITE	2.4%	3.2%	3.0%	3.5%	3.7%
SECONDRY(<57%) ILMENITE	5.5%	6.0%	2.4%	5.7%	9.4%
Ti-MAGNETITE (<5%TiO ₂)	0.0%	0.0%	0.0%	0.0%	0.0%
FE-OXIDE	0.0%	1.5%	1.4%	1.9%	3.1%
ZIRCON	1.2%	0.4%	1.8%	0.0%	2.3%
MONAZITE	0.0%	0.0%	0.0%	0.0%	0.0%
ALUMINO-SILICATE	1.3%	0.3%	0.9%	1.6%	0.6%
APATITE	3.0%	3.4%	2.9%	4.3%	6.1%
CHLORITE	2.3%	0.6%	0.4%	0.4%	0.0%
BIOTITE	2.4%	0.0%	0.0%	0.4%	0.0%
MUSCOVITE	6.8%	0.8%	3.0%	1.7%	0.0%
GARNET	4.4%	4.1%	6.6%	10.8%	9.3%
EPIDOTE	5.8%	8.0%	8.0%	9.6%	9.5%
SPHENE	3.1%	1.6%	4.9%	2.5%	3.1%
STAUROLITE	0.5%	1.4%	0.5%	0.5%	0.7%
TOURMALINE	2.1%	2.2%	0.0%	1.9%	1.6%
AMPHIBOLE AND PYROXENE	53.5%	62.2%	60.8%	48.6%	47.5%
XENOTIME	0.6%	0.0%	0.0%	0.0%	0.0%



